Acoustic wave propagation in underwater shallow channel environments

I. J. G. Scott and D. de Cogan

Abstract— **Previous attempts to model acoustic propagation in a shallow underwater channel using Transmission Line Matrix (TLM) have been hampered by shortfalls in the basic formulation of an otherwise competent numerical modelling technique. Significant advances have been made in recent years and it is now possible to demonstrate the benefits of TLM in this application. Perfectly matched boundaries to limit the computation size to a specific area of interest are one of these advances. After introducing details of the TLM method we proceed to model a number of scenarios which describe acoustic propagation in an open finite channel of ocean. We confirm the need for an accurate boundary-conforming description and demonstrate why mesh refinement strategies are not appealing in this situation. Our approach can be used to account for the distortions in the received signal in an underwater channel and we highlight the influence of both surface state and receiver position.**

Index Terms— **numerical modeling, underwater acoustics**

I. Introduction

The majority of underwater numerical simulations rely on a flat surface approximation to the sea-air interface. One particular example of this is illustrated by the work of Buckingham and Tolstoy [1]. Their model of an offshore continental slope, although accurate mathematically, simplifies the sea-air interface considerably. The application of the TLM numerical method to general problems in underwater acoustics was described by Coates et al [2]. It was originally developed for electromagnetic problems by Johns and Beurle [3]. However, the first serious investigation of modelling a finite section of open ocean using TLM was described by Willison [4] in his PhD thesis. At the time the arbitrary placement of bounding walls was not possible due to the discrete nature of the TLM mesh, meaning his experiments had to rely on a stepped approximation to the curved boundaries of waves on the ocean surface. This stepped approach introduced new errors not seen in the flat surface approximations previously used for ocean modelling. A second problem arose in both the flat and stepped surface approximations. Computational storage limitations dictate the need for a finite model of what is essentially an open-bounded problem in two or three spatial dimensions. It is necessary to define absorbing boundary conditions to allow a section of a larger ocean body to be modelled. A TLM formulation of a distortionless absorbing boundary (known as a Perfectly Matched Layer or PML) has recently been developed and, when fall-off profiles are suitably described, can reduce the return signal to better than -40dB [5].

A requirement for accurate modelling in specialist applications has given rise to renewed interest in boundary conforming schemes in TLM. Chief amongst these is a recursive definition proposed by Mueller et al [6]. This approach, while limiting in time and space, achieves much higher error tolerances than a stepped approximation to an identical scenario [7]. However, the recursion which is involved limits the size of the computational space and can greatly increase the computational requirements of the TLM routine. For this reason an alternative approach, first proposed in [7] and validated for an electromagnetic problem, will be outlined within the acoustics context in section 2 of this paper.

The paper will begin with a review of the TLM numerical modelling method. This will be followed by a presentation of our boundary conforming scheme, which attempts to address some of the shortfalls of the approach of Mueller et al. Our approach will then be used in a series of shallow-water channel propagation experiments, which will demonstrate the computational benefits.

II. TRANSMISSION LINE MATRIX MODELING

TLM is a time-domain modelling technique which describes a physical problem by means of an electrical network analogue which includes sections of lossless transmission lines which provide both spatial and temporal discretisation. A lossless transmission line is a physical object which in electrical terminology can be thought of as an inductance in series and capacitance in parallel measured per unit length. These measures are usually given as L_d and C_d respectively, allowing the velocity or propagation speed of a signal on the line to be represented as

$$v = \frac{1}{\sqrt{L_d C_d}} \tag{1}$$

Since this line is lossless, no degradation of the signal is experienced, and hence the energy within a matrix formed from an assembly of lossless sections of transmission line will remain constant. The electromagnetic formula to describe the

Manuscript received November 13, 2006.

I. J. G. Scott, was an undergraduate student at the School of Computing Sciences, University of East Anglia, Norwich, NR4 7TJ, U.K. when this work was undertaken. He is now a research student (PhD) at the University of Nottingham, U.K.

D. de Cogan has retired from the School of Computing Sciences, UEA, Norwich, NR4 7TJ, U.K. and is currently teaching at SBC/USST, Shanghai, PRC

observed impedance is defined as $\sqrt{\frac{L_d}{C_d}}$.

From classical electromagnetics (or acoustics) we know that for a line of intrinsic impedance Z_0 where a load impedance Z_L is separated from an observer at the input by a length l_A we can describe the impedance which the observer perceives as

$$Z_{obs} = Z_0 \left[\frac{Z_L + Z_0 \tanh(\beta l_A)}{Z_0 + Z_L \tanh(\beta l_A)} \right] \quad (2)$$

where $\beta = 2\pi / \lambda$.

When the load impedance is equal to the intrinsic impedance, all energy injected into the system at the point of observation passes into the load; the system is matched. However when they are not equal, then a component of the input will be reflected and the magnitude, known as *reflection coefficient* is given by

$$\rho = \frac{Z_L - Z_0}{Z_L + Z_0} \quad (3)$$

While the key concept in the Johns and Beurle [3] approach to modelling signal propagation on a network of transmission lines was revolutionary at the time, it presents no difficulty in this era of digital signalling processing. Any wave-form was imposed on the mesh as a train of impulses. In the nature of impulses, they travel independently, complying at all times with Eqn (3) and when several arrive in the same place at the same time, what is observed is their superposition.

Fig. 1 illustrates a 2D TLM node with interconnecting finite sections of lossless transmission line obeying the properties so defined. For ease of identification of the direction of travel of impulses we use the points of a compass. We also define 'incident *from*' (the figure shows incidence from the west) and 'scattered *to'*. A pulse travelling along the western arm in this figure will experience a discontinuity when it arrives at the intersection or node centre. As a 'terminating load' it will see three identical transmission lines and it will assume that they are of infinite length. Accordingly, it will see an effective total impedance of $Z_0 / 3$ and if we apply Eqn (3) above we will have $\rho = -0.5$. A signal of half the original amplitude, but with phase reversed is scattered back into the western arm. The transmission coefficient in this case can be calculated as $\tau = (1 - \rho) / 3$. Three impulses of half the original amplitude and with phase maintained are scattered to the north, south and east.

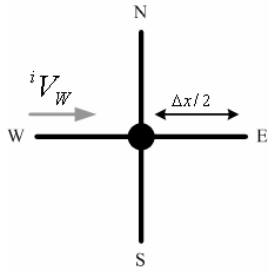

Fig. 1 - 2D TLM scalar node, with incoming pulse on west line

In our formulation, voltage pulses, the electrical analogue of acoustic pressure, have leading subscripts to denote direction and trailing superscripts to denote whether we are considering incident or scattered pulses. A trailing subscript is frequently used to designate iteration number.

At any discrete time-step of the iterative TLM procedure, the potential at the node can be calculated using the sum of the four currents divided by the sum of the admittances of the four interconnecting transmission line sections, as these are equal the formula can be simplified to give:

$$ {}_k\phi(x,y) = \frac{\left[\frac{2^iV_N}{Z_0} + \frac{2^iV_S}{Z_0} + \frac{2^iV_E}{Z_0} + \frac{2^iV_W}{Z_0} \right]}{\left[\frac{1}{Z_0} + \frac{1}{Z_0} + \frac{1}{Z_0} + \frac{1}{Z_0} \right]} = \frac{\left[{}^iV_N + {}^iV_S + {}^iV_E + {}^iV_W \right]}{2} \quad (4)$$

Individual incident pulses are scattered according to Eqn (3) and for the four directions in Fig. 1 this can be expressed as

$$\begin{pmatrix} {}^sV_N \\ {}^sV_S \\ {}^sV_E \\ {}^sV_W \end{pmatrix} = \frac{1}{2} \begin{bmatrix} -1 & 1 & 1 & 1 \\ 1 & -1 & 1 & 1 \\ 1 & 1 & -1 & 1 \\ 1 & 1 & 1 & -1 \end{bmatrix} \begin{pmatrix} {}^iV_N \\ {}^iV_S \\ {}^iV_E \\ {}^iV_W \end{pmatrix} \quad (5)$$

Individual pulses travel along their transmission lines during the discrete time interval (Δt) before arriving at adjacent nodes. The *connect* process describes what is incident at (x,y) at the new time (k+1) in terms of what was scattered from neighbours at the previous time (k) and is summarised as

$$\begin{aligned} {}_{k+1}{}^iV_N(x,y) &= {}_k{}^sV_S(x,y+1) \\ {}_{k+1}{}^iV_S(x,y) &= {}_k{}^sV_N(x,y-1) \\ {}_{k+1}{}^iV_E(x,y) &= {}_k{}^sV_W(x+1,y) \\ {}_{k+1}{}^iV_W(x,y) &= {}_k{}^sV_E(x-1,y) \end{aligned} \quad (6)$$

Full details can be found in the relevant literature. The original paper by Johns and Beurle [3] also provides a solid foundation for the more modern uses of TLM [8].

A. Impedance transformation boundary description

As can be seen from Figs. 1 and 2, the nodes within a finite TLM mesh contain adjoining pieces of discrete length sections

of transmission line. In order for the mesh to remain stable and time to remain discrete within the simulation, the sections of transmission line must exist in discrete multiples of $\Delta x/2$. A signal scattered from a node travels this distance during time $\Delta t/2$ before it transfers from its cell to the cell of a neighbour. It then takes a further $\Delta t/2$ before it arrives at that node. For conventional formulations boundaries are placed at a distance $\Delta x/2$ from a node. A pulse which leaves a node next to a pressure release boundary will return to

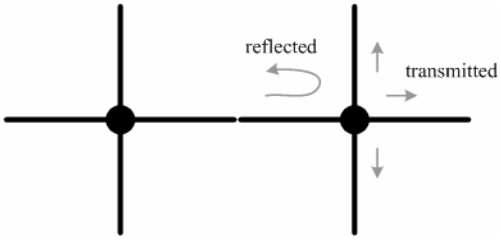

Fig. 2 - Scattering of pulse to neighbouring node in 2D TLM mesh

the same node with its phase reversed at that end of one discrete time-step. For the internal nodes in realistic problems this restriction does not present a difficulty.

However as can be seen from Fig. 3 (which represents the top bounding wall of the simulation) the ocean wave will in places cut the transmission line before and after the $\Delta x/2$ line end. In traditional TLM and used primarily in the work of Willison [4] these boundaries would have been approximated with a stepped boundary as in Fig. 3(b). Note the removal of the nodes where the length to the wall is less than $\Delta x/2.$ Other schemes are also possible, for example rounding all lengths up.

While this is widely used and commonly acceptable, the stepped approach to boundary definition can introduce large

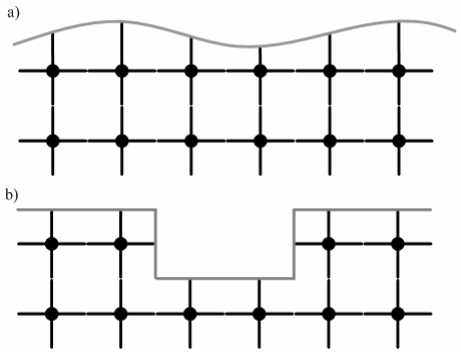

Fig. 3 - a) Non-uniform bounding wall of 2D TLM computation space, wall/wave is shown intersecting transmission line sections at non-discrete intervals, b) stepped approximation to same boundary

errors depending on the resolution of the mesh. In general, mesh refinement can help counteract these errors. However the computational requirements of the simulation will increase significantly. One attempt to circumvent this problem was proposed by Mueller et al [6] however the recursive nature of the definition proved almost as limiting, although the accuracy of the simulation was improved slightly. We will propose another technique which attempts to improve on the accuracy of the Mueller et al solution while increasing the efficiency by removing the need for recursion.

If we begin by placing an observer at the node, as in Fig. 4, the impedance observed from the node can be described by Eqn (2). However if we assume a low frequency model, as is normal for a TLM simulation, then the intrinsic impedance of the line can be represented as

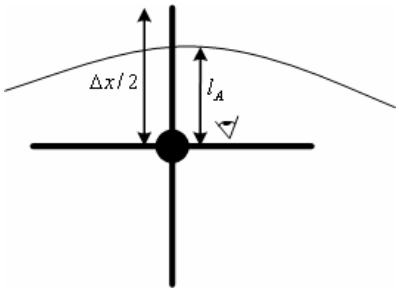

Fig. 4 - Observer looking toward boundary from node 'sees' identical impedance (observed impedance) regardless of length of line

$$Z_0 = \frac{\Delta t/2}{C_d \Delta x/2} = \frac{\Delta t'}{C_d l_A} \tag{7}$$

where C_d is the distributed capacitance of the line. This shows that it is possible to replace a line of length $\Delta x/2$ and impedance Z_0 with an equivalent line of length l_A. However the time to traverse the line is then changed, for this reason we cannot simply make this substitution within the TLM simulation as the discrete time nature would be lost. We can however adjust the intrinsic impedance of the line in Eqn (7) to compensate for the change in length, then the time Δt can remain constant, allowing the nature of the simulation to remain intact. This forms the basis of our approach.

If we assume a short circuit (pressure release) condition at the boundary, we can simplify Eqn (2) to give

$$Z_{obs} = Z_0 \tanh(\beta l_A) \tag{8}$$

however if we intend to replace this line with an equal line of length $\Delta x/2$ with transformed impedance Z_A, then

$$Z_{obs} = Z_A \tanh(\beta \Delta x/2) \tag{9}$$

Since a pulse incident on the line will observe the same impedance irrespective of the length of the line, equations (8) and (9) must equate to one another, therefore

$$Z_0 \tanh(\beta l_A) = Z_A \tanh(\beta \Delta x/2) \tag{10}$$

In its current form this is untidy to solve for Z_A. However upon closer inspection we see that if we make the low frequency assumption upon which TLM is founded, then the hyperbolic tangent can be replaced with its argument and

therefore Eqn (10) becomes

$$Z_0 \beta l_A = Z_A \beta \Delta x / 2 \tag{11}$$

simplifying and solving for Z_A gives

$$Z_A = Z_0 \left[\frac{2 l_A}{\Delta x} \right] \tag{12}$$

This very simple formula allows us to describe the non-uniform bounding walls of the computation space with an increased accuracy than was previously possible. Making this transformation on the impedances of the sections of transmission line meeting with the top ocean wave of the simulation allows an accurate description of the wave, with no extra computational overhead, or sophistications to the TLM iterative procedure itself.

It is also possible to describe a rigid boundary using this

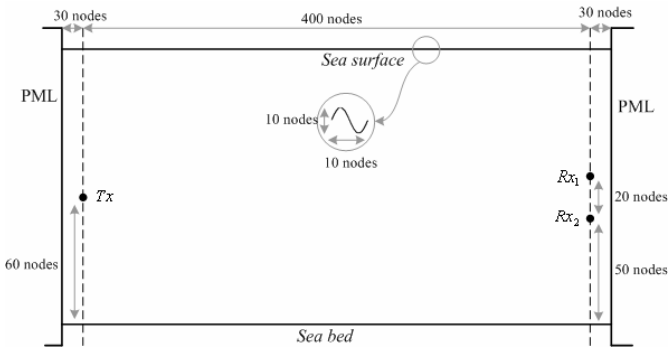

Fig. 5 - Section of wavy ocean, sinusoid of wavelength 10 nodes used to describe the ocean wave

same technique, for this boundary the load impedance, Z_L would tend toward infinity, giving Eqn (2) for 'normal' and transformed cases, after simplification

$$Z_{obs} = \frac{Z_0}{\tanh(\beta l_A)} \quad \text{and} \quad Z_{obs} = \frac{Z_A}{\tanh(\beta \Delta x / 2)} \tag{13}$$

making the low frequency assumption, equating and simplifying as before

$$Z_A = Z_0 \left[\frac{\Delta x}{2 l_A} \right] \tag{14}$$

Although this will not be specifically required for the ocean simulation, as the sea floor lands on discrete multiples of the mesh anyway, it is included here for completeness. These two simple formulae, unlike the Mueller et al approach, also allow a bounding wall to cut before the $\Delta x / 2$ line end, this occurs because of the placement of the reference plane at the node as apposed to the $\Delta x / 2$ line end which is used in the Mueller et al approach.

The remainder of this paper will utilise this scheme, showing the benefits of such an approach in a practical situation, while also indicating the need for accurate boundary descriptions within TLM simulations.

III. ACOUSTIC PROPAGATION IN A SHALLOW CHANNEL

The approach used by Wilison [4] to treat the shallow-water problem started by defining a 2D section of the ocean to be modelled as in Fig. 5. The top boundary was defined with a refection coefficient ρ = -1, while the bottom was defined as a rigid boundary, i.e. $\rho = 1$. In our repetition of this work a single shot-pulse was injected at the transmitter position (labelled T_x) and was allowed to propagate throughout the mesh during 1000 iterations. The signals were allowed to scatter between the sea-bed and the sea-surface, which was defined as a sinusoid wave with peak-to-peak amplitude and wavelength of 10 nodes ($\Delta x = 0.5m \therefore 10 nodes = 5m$).

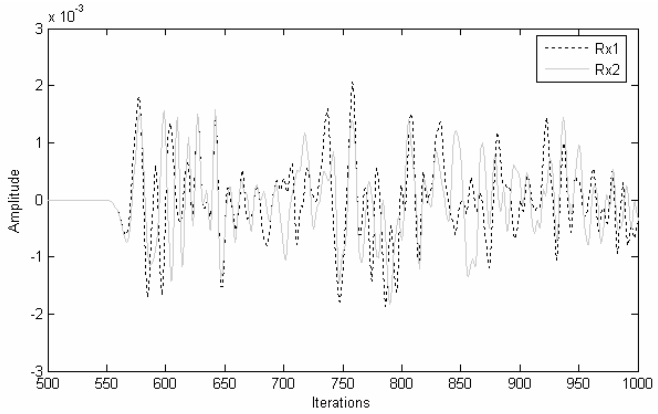

Fig. 6 - Signal received at receiver locations indicated in Fig. 5 after 1000 iterations, with stationary sinusoidal ocean wave, broken = Rx_1, continuous = Rx_2

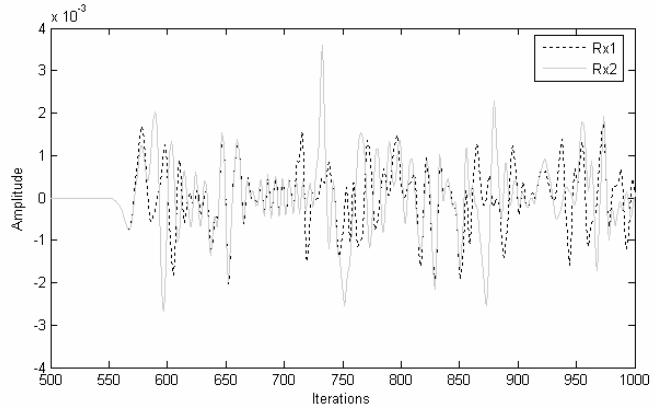

Fig. 7 - Signal received at receiver locations indicated in figure 5 after 1000 iterations, with flat ocean wave, broken = Rx_1, continuous = Rx_2

This stretched for a total of 400 nodes along the top surface and into our distortionless matched-load regions which bounded our computational space to the left and right in the figure. The time-domain response was monitored at positions Rx_1 and Rx_2. An example of the received signal is shown in Fig. 6. This can be compared with the results of Fig. 7, which show a similar scenario using a flat surface. The surface topography quite clearly has an influence.

Interesting though this may be it should be remembered that in a real underwater acoustic channel the surface boundary will not be stationary, in fact its character will depend on ocean currents, depth, windage and fetch. We can include this in the simulation by moving the top wave after each injection of a pulse. This is possible due to the relative differences in velocity of the propagating acoustic wave and the sea surface. As sound travels at approximately 1500m/s in sea water and the fastest ocean waves typically travel around 150m/s (e.g. a tsunami). For normal ocean conditions wave velocity is much slower. So, the sound wave within the water channel has a velocity which can be orders of magnitude faster than any sea-surface fluctuation. This means that the signal reaching and interacting with the surface will perceive it as effectively stationary upon each iteration. This allows us to create a 3D view of time against iterations within the simulation. If we repeat this for the same scenario depicted by Fig. 5 for the movement of one complete wavelength of the top wave, moving at a speed of 1 node every 10 steps in time. The results in Fig. 8, which are generated during 1500 iterations confirm that the received signal is strongly dependent on the current position of the top wave. As can also be seen there is an almost sinusoidal nature of the signal moving forward in time, in comparison to that of the top surface. To allow the data to be interpreted easier, the situation result has been smoothed by convolving the 2D matrix holding the values, with a 2D Gaussian mask defined by

$$g(x,y) = \frac{1}{2\pi} e^{-\left[\frac{x^2+y^2}{2}\right]} \tag{15}$$

centred around 0 and with standard deviation of 1. The receiver closer to the sea-surface exhibits much larger fluctuations in received signal than that closest to the sea floor.

The simulation can be repeated for a variety of sea-surface descriptions. A number of these will be demonstrated at the conference.

As a comparison we model a flat ocean surface most commonly assumed in oceanographic simulations, generating the results of Fig. 9. As can be seen, at each instant in time the propagating signal will see the top wave in an identical position (the movement has no effect as the surface is identically flat across its entirety), hence no distortions except those caused by the reflections from the surface are observed. This indicates the level of error already incorporated within a smooth surface ocean model. Dependant on the depth of receiver, transmitter and ocean segment, this may be acceptable in some circumstances, for example deep ocean transmissions where the surface has little effect, however for shallow channels, perhaps those around shipping lanes and close to port, it is necessary to incorporate the sea-surface into the model.

IV. SEA-SURFACE DIFFRACTION PROPERTIES

One possible explanation to account for some of the distortions seen at the received signal is found by observing the 2D propagation of a sinusoidal point source within an

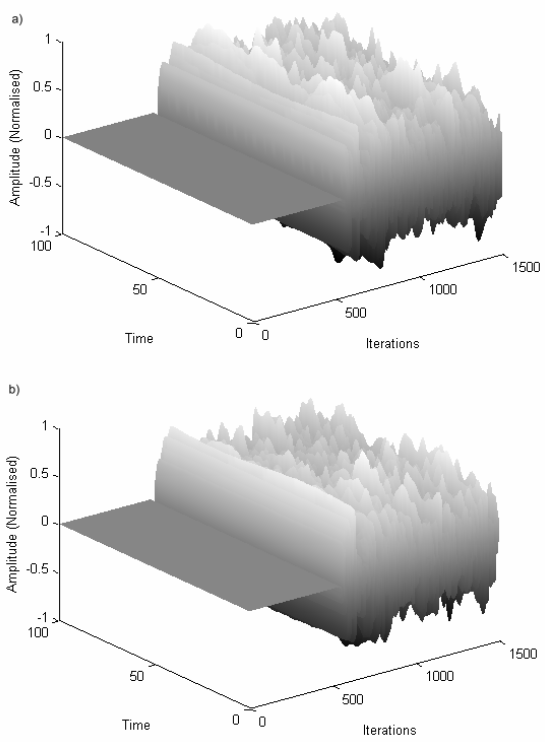

Fig. 8 - a) 3D plot of received signal at Rx_1, b) 3D plot of received signal at Rx_2, for a sinusoid shaped ocean wave of wavelength 10 nodes and peak-to-peak amplitude of 10 nodes, smoothed with a 2D convolution with the Gaussian function

identical environment. To elaborate the properties of interest, the top ocean topography was arranged as a set of conidial-like waves (approximated by a set of x^2 type curves) with a peak-to-peak distance of 150 nodes with a peak-to-trough amplitude of 40 nodes. Six repeats of the basic structure were placed on top of an ocean channel where the wave trough to sea bed distance comprised 200 nodes. A sinusoidal point-source was positioned 100 nodes below the level of wave

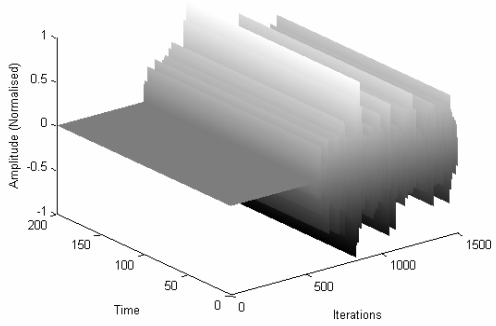

Fig. 9 - Plot of received signal at Rx_1, for a flat ocean wave

troughs and is located 800 nodes along the horizontal (see Fig. 10). Simulations were run for input signals of different frequencies. We started with the case where the wave-length injected at the point of excitation was 250 nodes, i.e. significantly longer than the surface-wave peak-to-peak

distance. The results, shown in Fig. 10a confirm that the surface topography does influence the wave distribution in the horizontal direction. The wave distribution in the vertical direction is also distorted. The situation when the wavelength of the excitation is 200 nodes is shown in Fig. 10b. The diffraction patterns when the wavelength is reduced to 100 nodes are shown in Fig. 10c. At $\lambda = 50$ nodes there is still some wave-like behaviour, but by the time we go to $\lambda = 20$ nodes we are within the ray-tracing domain, although, even here it seems the situation is complicated by surface topography.

V. CONCLUSIONS

In the course of this paper we have presented details of our modification to the basic TLM algorithm for describing zero displacement and pressure release boundaries for acoustic propagation problems where such boundaries are not spatially uniform. This enhancement allows us to create surface conforming meshes that are more accurate than step-wise approximations and more computationally efficient than recursive formulations. Taken together with recent developments in TLM open-boundary descriptions, we have been able to model the shallow water acoustic channel problem more effectively than was previously possible using this numerical technique. The underwater acoustic channel in the presence of air/sea disturbances (sea-waves) is often described as being a multi-path propagation problem. Our work confirms that this is only true when the wavelength of the signals is significantly shorter than the peak-to-peak distance of surface waves. Receiving devices close to the sea surface register greater perturbations due to surface topography than those which are located much deeper. It can be seen in Fig. 10 that the nature of the surface still has a significant effect on the wave distribution just above the zero-displacement boundary. We have highlighted the fact that the underwater propagation channel represents a very interesting 'fast-slow' problem. The velocity of even the fastest surface wave is significantly less than the acoustic velocity in the aqueous medium. Thus, at any instant, a propagating signal 'sees' a fixed boundary, which will, of course, be different at any other instant. We have demonstrated the diffraction effects on signals of different wavelengths. Although it has not formed part of our presentation in this paper, it is quite clear that a fixed frequency emitted by the source will be perceived at the receiving point as having a time-varying amplitude which is affected by the surface wave peak-to-peak distance and the velocity component of that wave along the propagating path. The influence of these factors on the reception of real signals as a function of time can be easily simulated. Our work has concentrated on a constant velocity of propagation. In real situations insolation and/or meteorological conditions may cause the temperature of the water at the surface to be significantly different to that in the bulk. TLM can accommodate this using a modified nodal configuration which includes what is called a 'transmission line stub'. Details of the development of such algorithms may be found in section 4.8 of reference [8]. In particular, Fig. 4.19 in that reference demonstrates acoustic propagation in a stratified medium such as occurs during periods of meteorological temperature inversion.

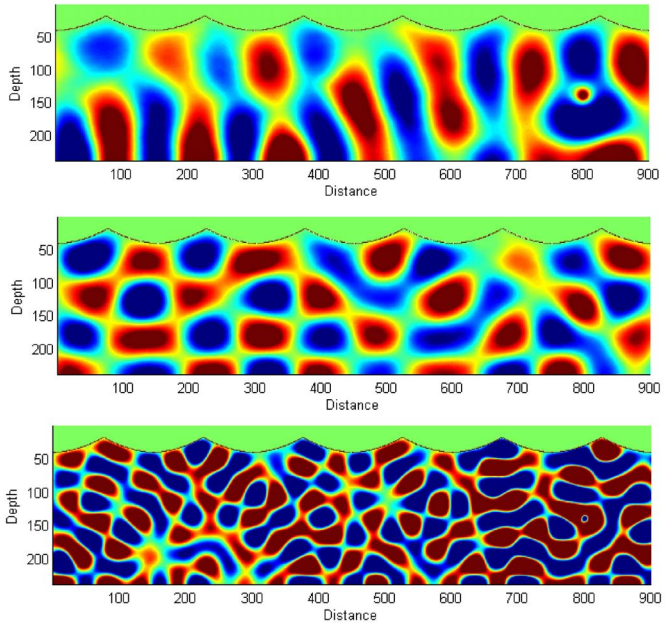

Fig. 10 - Surface plots of a sinusoidal point source propagating normal to surface waves with peak-to peak distance = 150 nodes in a shallow channel. *a*, to *c* from top to bottom: (a) $\lambda_{excitation} = 250$ nodes, (b) $\lambda_{excitation} = 200$ nodes, (c) $\lambda_{excitation} = 100$ nodes

REFERENCES

[1] M. J. Buckingham, A. Tolstoy, "*An analytical solution for benchmark problem 1: The 'ideal' wedge*", Journal of the Acoustical Society of America, April 1990, Vol. **87** (4),

[2] R. F. W. Coates, D. de Cogan, and P. Willison, "*Transmission line matrix modelling applied to problems in underwater acoustics"* Proceedings of International Oceans Conference, Washington DC, September '90

[3] P. B. Johns, R. L. Beurle, "*Numerical solution of 2-dimensional scattering problems using a transmission line matrix*", Proceedings of the IEE **118,** (1971), 1203-1208

[4] P. A. Willison, "*Transmission Line Matrix modelling of underwater acoustic propagation*", PhD thesis, University of East Anglia, Norwich, September 1992

[5] N. Peña, M.M. Ney, "*Absorbing-boundary conditions using Perfectly-Matched-Layer (PML) technique for three-dimensional TLM simulations*" IEEE Trans. on Microwave Theory and Techniques **MTT-45** (1997) 1749 - 1755

[6] U. Mueller, A. Beyer, W. J. R. Hoefer, "*Moving Boundaries in 2-D and 3-D TLM Simulations Realized by Recursive Formulas*", IEEE Trans. on Micro. Theo. and Tech., Vol. **40** (12) December 1992, 2267-2271

[7] I. J. G. Scott, D. de Cogan, "*Improved Mesh Conforming Boundaries for the TLM Numerical Method*", PIERS (Progress in Electromagnetics Research Symposium), Cambridge MA, March 2006, 336-343

[8] D. de Cogan, W. J. O'Connor, S. Pulko, "*Transmission Line Matrix Modelling in Computational Mechanics*", Taylor and Francis/CRC Press, Boca-Raton 2006

[9] I. J. G. Scott, D. de Cogan, "*An improved Transmission Line Matrix model for the Buckingham and Tolstoy benchmark test*", Submitted for publication in J. Acous. Soc. Am., July 2006